Sakarya Üniversitesi Fen Bilimleri Dergisi
Sakarya University Journal of Science
e-ISSN : 2147-835X
Publisher : Sakarya University
Vol. 29, No. 6, 660-672, 2025
DOI: https://doi.org/10.16984/saufenbilder.1776359
Research Article

Comparative Investigation of the Microstructure, Hardness, and Tribological Properties of Electroless Ni–B Composite Coatings Reinforced with TiO_2 and ZrO_2

Deniz Gültekin

Sakarya University, Faculty of Engineering, Department of Metallurgical and Materials Engineering, Sakarya, Türkiye, dkurt@sakarya.edu.tr, ror.org/04ttnw109

ARTICLE INFO

Keywords:
Electroless Ni–B coatings
Composite
Microstructure
Microhardness
Tribology

Article History:
Received: 02.09.2025
Revised: 23.09.2025
Accepted: 01.10.2025
Online Available: 12.12.2025

ABSTRACT

This study focuses on the electroless deposition and characterization of Ni–B composite coatings reinforced with TiO_2 and ZrO_2 ceramic particles. Coatings were deposited on steel substrates using an acidic bath ($NiSO_4 \cdot 6H_2O$, DMAB, thiourea, sodium acetate) under controlled conditions (65 ± 3 °C, pH 6, 350 rpm, 45 min) with reinforcement contents of 0 to 15 g/L. The coatings were systematically evaluated in terms of morphology, structure, hardness, and tribological performance. Ni–B exhibited the typical nodular morphology, while the incorporation of TiO_2 and ZrO_2 progressively modified surface features. At moderate concentrations, both reinforcements were uniformly dispersed within the matrix, whereas higher contents led to particle clustering and microstructural heterogeneity. XRD confirmed the amorphous–nanocrystalline nature of Ni–B; TiO_2 acted mainly as an inert phase, while ZrO_2 promoted localized crystallization, resulting in harder and more stable structures. Microhardness increased from ~750 HV for plain Ni–B to ~985 HV (TiO_2) and ~1080 HV (ZrO_2) at 10 g/L, with a slight decline at higher loadings due to agglomeration. Tribological tests demonstrated that both reinforcements improved wear resistance and reduced friction, with TiO_2 yielding more stable friction coefficients and ZrO_2 providing superior resistance to material loss. These results highlight the potential of TiO_2- and ZrO_2-reinforced Ni–B coatings as sustainable alternatives with improved mechanical and tribological functionality for engineering applications.

1. Introduction

Electroless plating, first developed following the Electroless coating technology, has emerged as a critical surface modification technique across diverse industrial sectors due to its ability to deposit uniform and adherent films on various substrates without requiring an external electrical current [1–4]. This autocatalytic process provides distinct advantages such as operation at relatively low temperatures, cost-effectiveness, and the capability to coat complex geometries and even non-conductive materials, making it a versatile method for enhancing surface properties [1, 2].

Among the wide range of electroless coatings, nickel-based systems have attracted particular attention due to their excellent combination of tribological, mechanical, and corrosion resistance properties [5, 6]. These coatings are widely applied in chemical processing industries, aerospace, automotive, electronics, and where components must operate under severe conditions [7]. For instance, electroless Ni–P coatings are well known for their high hardness and superior corrosion resistance, making them suitable for demanding applications [8, 9]. Recent studies have further indicated that electroless Ni–B coatings can exhibit even higher hardness and wear resistance than tool steels and hard chromium coatings, respectively [5, 10]. The mechanical performance of these coatings is

Cite as: D. Gültekin, "Comparative investigation of the microstructure, hardness, and tribological properties of electroless Ni–B composite coatings reinforced with TiO_2 and ZrO_2," Sakarya University Journal of Science, vol. 29, no. 6, pp. 660-672, 2025. https://doi.org/10.16984/saufenbilder.1776359

strongly dependent on the chemical composition—such as phosphorus or boron content—as well as post-deposition heat treatments, which can further enhance hardness and adhesion if carefully controlled [6, 11].
A major advancement in electroless coating technology has been the addition of ceramic reinforcements into the Ni-based matrix to produce composite coatings [12]. This approach aims to exploit the inherent hardness, chemical stability, and wear resistance of ceramics to reinforce the metallic matrix, thereby further improving the functional performance of electroless coatings [13–15]. A wide range of ceramic nanoparticles—such as SiC, ZrO_2, TiO_2, Al_2O_3, WC, and MgB_2—have been successfully co-deposited in Ni–based matrices [16–24]. These reinforcements improve coating hardness and wear resistance mainly through grain refinement and dispersion strengthening mechanisms, while also enhancing corrosion resistance in aggressive environments [25–28].

Electroless Ni–B coatings, originally developed after the pioneering work of Brenner and Riddell, are of particular interest due to their potential to replace toxic hard chromium coatings [9]. Conventional Ni coatings generally possess hardness values of approximately 450 HV, whereas Ni–B coatings, particularly after heat treatment, can attain values approaching 1000 HV. This remarkable increase translates into enhanced hardness, improved wear resistance, and greater chemical stability, making them highly suitable for demanding engineering applications [10]. To further enhance their performance, ceramic particles such as SiC, TiO_2, Al_2O_3, and ZrO_2 have been incorporated into Ni–B matrices. Prior studies have reported that TiO_2 reinforcement improves microhardness and stabilizes frictional behavior [15, 17], while ZrO_2 contributes to refined morphology and superior wear resistance [18, 19]. In addition to Ni–B–W coatings, research has also investigated various reinforcement additions and bath compositions—for example, Ni–B–W–SiC systems—where optimization of both electrolyte formulation and mechanical/tribological performance has been emphasized [23, 29–31].

Despite these advantages, the concentration and distribution of reinforcement particles remain critical. Excessive particle loading can cause agglomeration in the bath and produce heterogeneous coatings with reduced mechanical performance [4, 24, 32]. Furthermore, conventional electroless baths often rely on toxic stabilizers such as lead or thallium, which pose environmental hazards. Recent research has therefore shifted toward more sustainable, environmentally friendly electroless baths, which offer high performance without compromising ecological safety [4, 8].

Within this framework, the present study focuses on a comparative evaluation of TiO_2- and ZrO_2 reinforced Ni–B composite coatings deposited using a lead-free acidic bath. The objective is to systematically investigate how reinforcement type and concentration influence the microstructure, microhardness, and tribological performance of the coatings. The synergy of sustainable processing and ceramic particle reinforcement explored in this study contributes to the development of durable electroless composite coatings with potential for advanced engineering applications.

2. General Methods

Electroless Ni–B and ceramic particle-reinforced Ni–B coatings were deposited on low-carbon steel substrates using an acidic bath, which has been reported to enhance coating adhesion and reduce environmental concerns [4]. The process is schematically illustrated in Figure 1. Bath components and conditions are summarized in Table 1.

Table 1. Bath composition and operating conditions for electroless Ni–B and Ni–B/ceramic composite coatings

Bath Composition	Concentration (g/L)
Nickel sulfate hexahydrate	30
DMAB	3
Thiourea	0.05
Sodium acetate	4.5
TiO_2	0, 2.5, 5, 10, 15
ZrO_2	0, 2.5, 5, 10, 15
Operating Conditions	**Value**
Temperature (°C)	65
pH	6
Stirring speed (rpm)	350
Time (min)	45

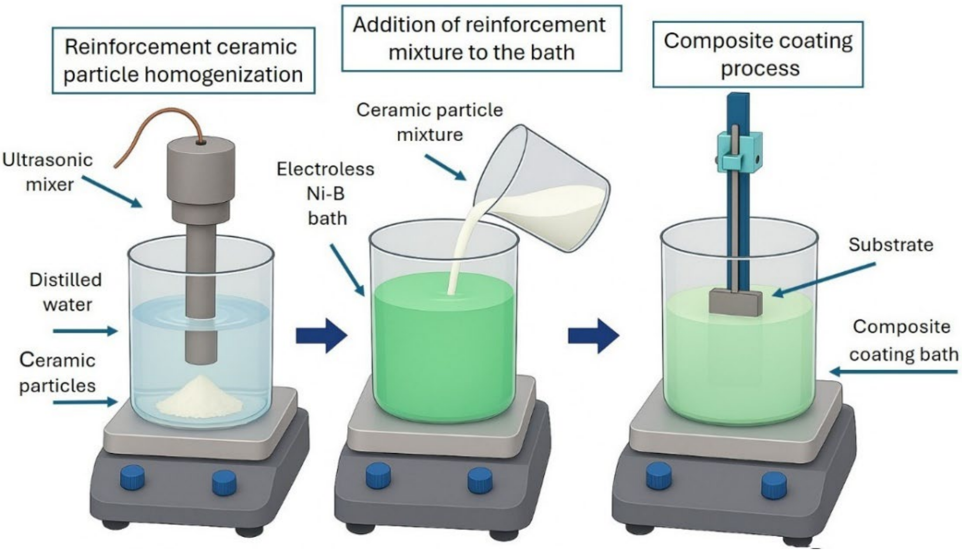

Figure 1. Schematic illustration of the electroless Ni–B/ceramic composite coating process. (The figure was drawn by the author, inspired by previous work [4])

Prior to deposition, steel substrates were prepared through a multi-step surface treatment. Substrates were mechanically cleaned by using SiC papers (200-1200 grit), followed by alkaline cleaning in a 5% sodium hydroxide solution for 10 minutes. The samples were surface activated by immersion in 50% HCl for 30 seconds, followed by rinsing with distilled water. The bath composition consisted of nickel sulfate hexahydrate ($NiSO_4 \cdot 6H_2O$, 30 g/L) as the Ni^{2+} source, dimethylamine borane (DMAB, $(CH_3)_2NHBH_3$, 3 g/L) as the reducing agent sodium acetate (CH_3COONa, 4.5 g/L) as the complexing agent, and thiourea (CH_4N_2S, 0.05 g/L) as the stabilizer as previously described in Ref. [4]. The bath was maintained at pH 6–6.5 and 65 ± 3 °C for 45 min to ensure stable deposition and homogeneous particle incorporation. For the composite coatings, TiO_2 and ZrO_2 nanoparticles were separately incorporated into the bath at concentrations of 0 to 15 g/L. The particles were ultrasonically dispersed in distilled water containing sodium dodecyl sulfate (SDS, 0.5 g/L) before the addition to ensure homogeneous distribution within the electrolyte. In addition, a reference Ni–B coating without ceramic reinforcement was also produced under identical conditions for comparison. Following deposition, SEM coupled with EDS was employed to investigate the surface features and elemental composition of the coatings. Structural and crystallographic information was obtained through XRD analysis using Cu-Kα radiation. Microhardness was measured with a Vickers indenter to determine the effect of ceramic additions on mechanical strength. Dry sliding wear tests were conducted on a pin-on-disc tribometer, employing a 6 mm Al_2O_3 ball as the counterface. The tests were carried out at 0.4 m/s sliding speed, 5 N load, over a total distance of 200 m. Post-test, worn surfaces were inspected via SEM to identify dominant wear mechanisms and associate them with friction and wear rate results.

3. Results and Discussion

3.1. Morphological and compositional analysis

Figure 2 shows the SEM and EDS analyses of the plain Ni–B coating produced under the same bath conditions as the composites. The coating shows a typical cauliflower-shaped nodular surface, which is a distinctive feature of electroless Ni–B deposits and arises from rapid nucleation and growth processes under high overpotential conditions [4]. XRD results also confirmed the presence of a broad Ni (111) peak, indicating an amorphous to nanocrystalline structure, consistent with previous reports [4, 9, 10]. Figures 3 and 4 present the morphological evolution of Ni–B coatings reinforced with TiO_2 and ZrO_2, respectively. At low reinforcement contents (2.5 g/L), TiO_2 particles appeared as fine bright contrasts embedded within the nodular matrix without disturbing surface uniformity. As the content increased to 5 g/L, more particles accumulated at nodule boundaries, slightly reducing homogeneity. At 10 g/L, clustering became evident, and the compact nodular morphology partially disappeared, giving way to a rougher and heterogeneous surface.

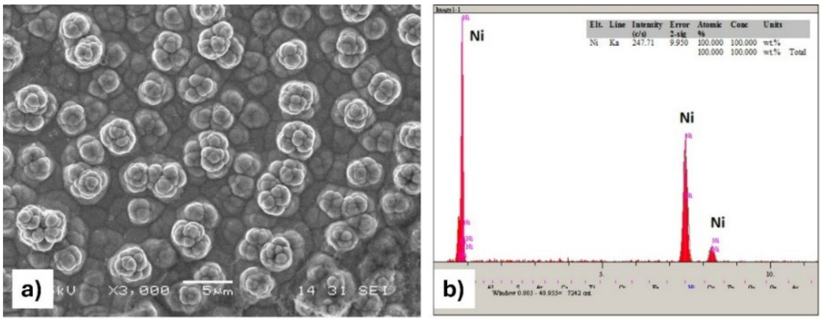

Figure 2. Surface morphology and chemical composition of the plain Ni–B coating: (a) SEM micrograph showing the characteristic nodular morphology, (b) corresponding EDS spectrum

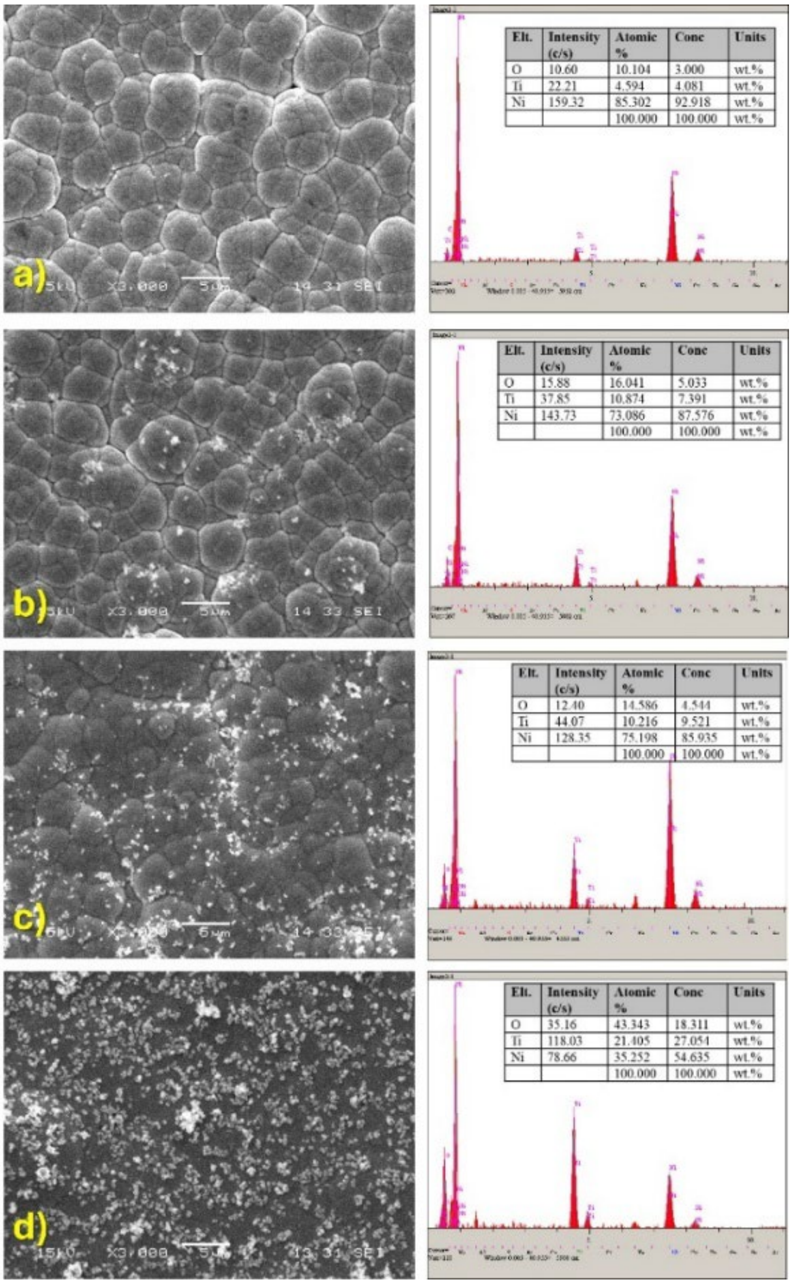

Figure 3. SEM micrographs and EDS spectra of Ni–B/TiO_2 composite coatings produced with different particle concentrations: (a) 2.5 g/L, (b) 5 g/L, (c) 10 g/L, (d) 15 g/L

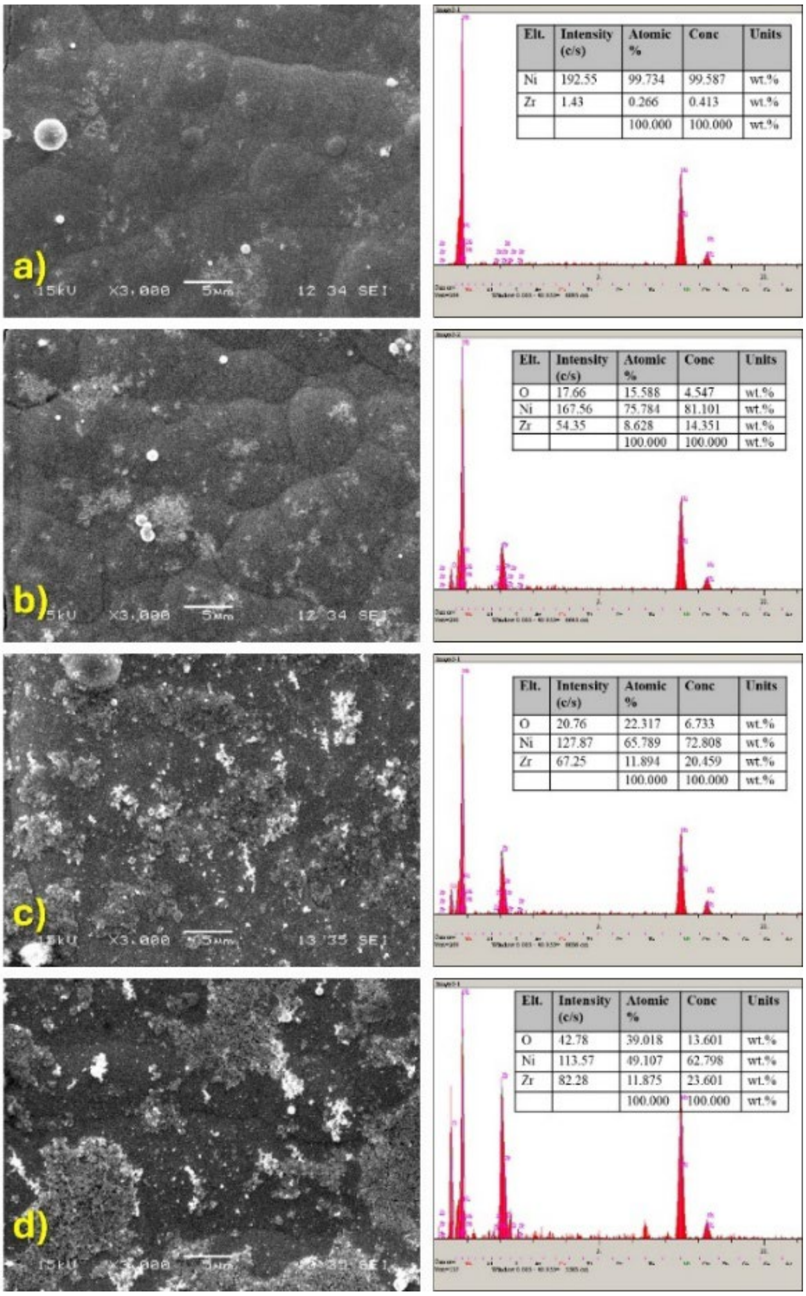

Figure 4. SEM micrographs and EDS spectra of Ni–B/ZrO_2 composite coatings at different reinforcement levels: (a) 2.5 g/L, (b) 5 g/L, (c) 10 g/L, (d) 15 g/L

At the highest content (15 g/L), the nodular morphology was almost completely replaced by dense particle agglomerations, resulting in disrupted matrix continuity. EDS spectra supported these observations, showing progressive increases in Ti and O signals with higher reinforcement levels. A similar trend was observed in ZrO_2-reinforced coatings (Figure 4), though particle size and distribution characteristics differed from TiO_2. At 2.5 g/L, ZrO_2 particles were sparsely embedded in the nodular surface, with minimal distruption. At 5 g/L, localized accumulations began to form, increasing surface roughness. At 10 g/L, the nodule boundaries were almost obscured by particle clusters, and at 15 g/L, the surface was dominated by ZrO_2 agglomerates, causing loss of nodular integrity. Compared with TiO_2, ZrO_2 particles displayed a stronger tendency to agglomerate, producing irregular topographies even at intermediate loadings. EDS confirmed the gradual enrichment of Zr and O peaks with increasing reinforcement. Increasing TiO_2 content leads to progressive particle incorporation and agglomeration. These results indicate that particle incorporation alters the nodular morphology of Ni–B coatings in a concentration-dependent manner. Low additions preserve matrix continuity while providing embedded reinforcements, whereas high additions lead to agglomeration and rough heterogeneous surfaces, which can negatively affect coating integrity.

The cross-sectional SEM images and corresponding EDS spectra of Ni–B (a), Ni–B/TiO_2 (b), and Ni–B/ZrO_2 (c) coatings are presented in Figure 5. The plain Ni–B coating exhibited a dense and uniform layer with an average thickness of ~12.4 μm, and EDS confirmed the expected Ni-rich composition without detectable impurities. For the TiO_2-reinforced coating (b), a thickness of ~9.4 μm was measured, and the incorporation of Ti was clearly confirmed by EDS analysis (7.7 at. % Ti, 2.9 wt.% O). The coating retained good structural integrity, although the presence of reinforcement particles slightly increased interfacial roughness. This suggests that TiO_2 particles were successfully embedded within the Ni–B matrix and contributed to local heterogeneity, consistent with the improved hardness values reported.

The ZrO_2-reinforced coating (c) exhibited a thickness of ~11.6 μm, and EDS analysis verified the incorporation of Zr (11.9 at. % Zr, 6.7 wt.% O). Compared to the TiO_2 system, ZrO_2 addition resulted in more pronounced particle incorporation and localized variations across the cross-section, which is in agreement with the XRD results showing partial crystallization. Despite these microstructural heterogeneities, the coating-maintained continuity without visible delamination, indicating sufficient adhesion to the substrate. Overall, cross-sectional analyses confirmed that both TiO_2 and ZrO_2 nanoparticles were effectively incorporated into the Ni–B matrix, though their distribution and influence differed depending on the reinforcement type.

3.2. Phase structure and crystallinity

The phase composition of plain Ni–B and Ni–B composite coatings was examined by X-ray diffraction (Figure 6). The reference Ni–B coating exhibited broad reflections corresponding to fcc-Ni (111), (200), and (220) at approximately 44.4°, 51.7°, and 76.3°, respectively (JCPDS 01-087-0712).

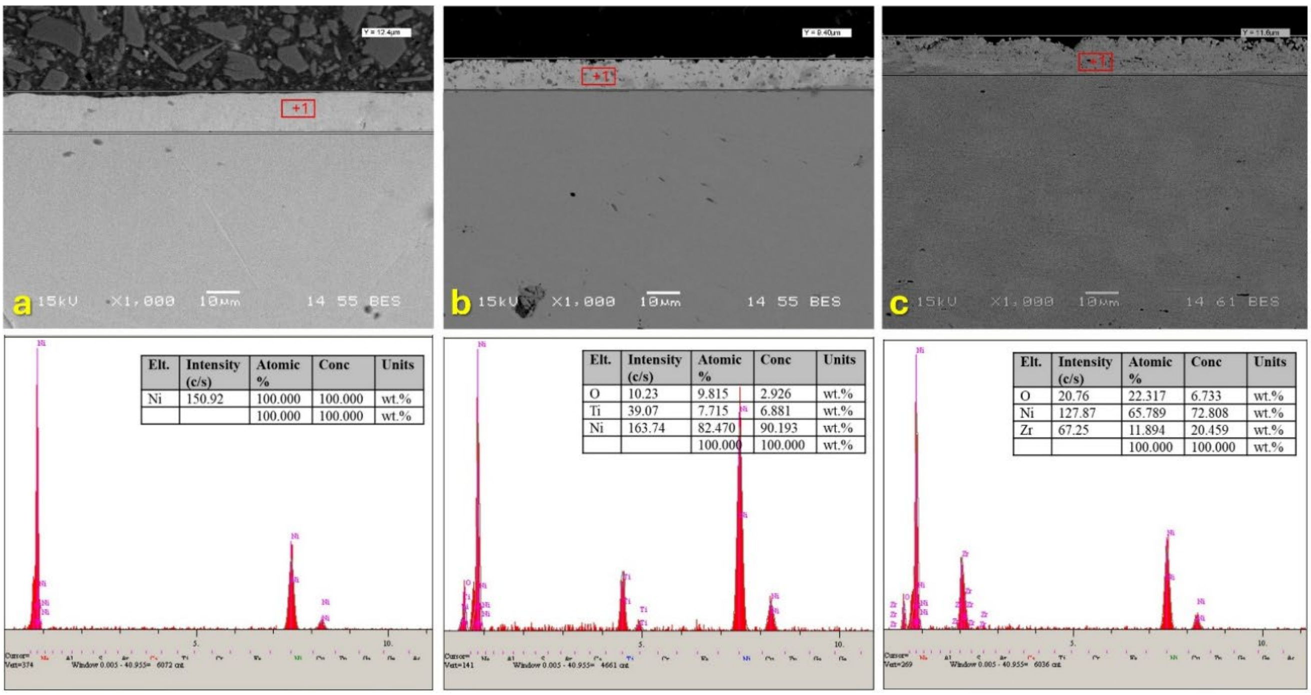

Figure 5. Cross-sectional SEM images and corresponding EDS spectra of (a) Ni–B, (b) Ni–B/TiO_2, and (c) Ni–B/ZrO_2 coatings

The broad and low-intensity nature of these peaks indicates the presence of an amorphous to nanocrystalline structure, resulting from the incorporation of boron into the Ni lattice, which disrupts long-range atomic ordering. Such amorphous or partially crystalline features are frequently reported for electroless Ni–B coatings deposited at relatively low temperatures [4, 3, 10].

For TiO_2-reinforced coatings, low particle concentrations (5 g/L) produced only broadening of the Ni reflections, without introducing significant secondary peaks. A weak signal near 25° was associated with the rutile TiO_2 phase (ICDD 00-021-1276). At 10 g/L, rutile peaks at ~27.4°, 36.0°, 54.0°, and 63.0° became evident, though no distinct shift was observed in the Ni peaks, confirming that TiO_2 particles acted mainly as inert embedded phases rather than reacting chemically with the Ni–B matrix. At the highest reinforcement (15 g/L), rutile reflections intensified, but the amorphous Ni–B character remained dominant, consistent with SEM results that showed extensive surface particle accumulation.

In contrast, ZrO_2-reinforced coatings exhibited more pronounced structural effects. At 5 g/L, additional weak peaks were observed, corresponding to tetragonal ZrO_2 near 30–31° and monoclinic ZrO_2 near 28°. Increasing the content to 10 g/L intensified these reflections, while the Ni (111) peak at ~44.5° became sharper, indicating partial crystallization of the matrix. At 15 g/L, tetragonal and monoclinic ZrO_2 peaks became dominant, while the broad amorphous hump weakened, suggesting that ZrO_2 particles acted as heterogeneous nucleation sites and promoted crystallization.

These results highlight a fundamental distinction between the two ceramic reinforcements. TiO_2 behaved in a largely inert manner, being physically incorporated into the Ni–B matrix without exerting a significant influence on phase formation or structural refinement. This passive role is consistent with earlier reports, where TiO_2 was mainly observed to act as a dispersion-strengthening phase, enhancing hardness by particle reinforcement rather than altering the crystallization pathway [10, 14]. In contrast, ZrO_2 demonstrated a more active contribution by directly affecting the crystallization behavior of the Ni–B matrix. At higher loadings, ZrO_2 promoted increased crystallinity, which can be attributed to its heterogeneous nucleation capability and tendency to reduce local free energy barriers for crystal growth [29].

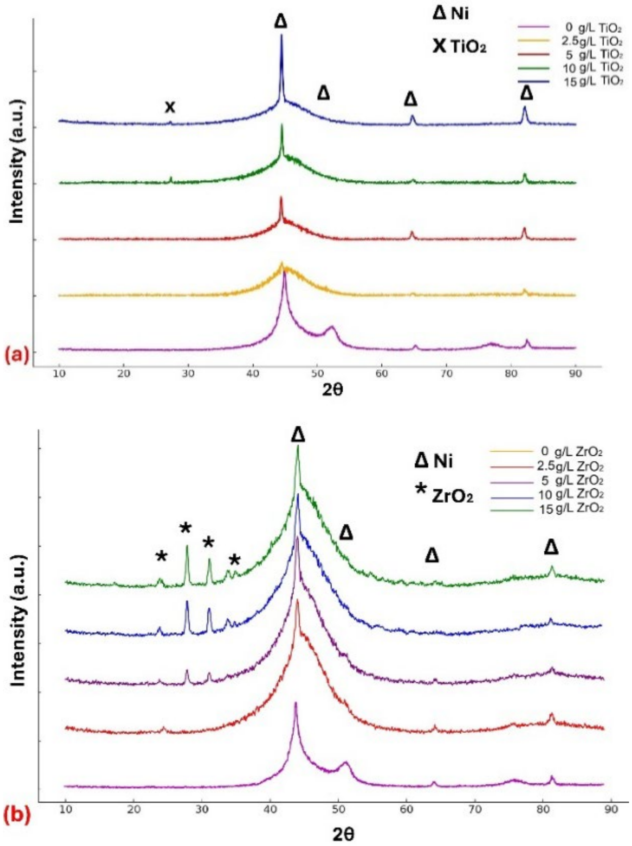

Figure 6. XRD patterns of electroless coatings: (a) Ni–B/TiO_2 composites, (b) Ni–B/ZrO_2 composites

This structural evolution correlates strongly with the SEM observations, where ZrO_2-containing coatings exhibited pronounced clustering and a greater impact on surface morphology compared to the relatively uniform dispersion of TiO_2. Such clustering is not not merely a morphological feature but reflects the stronger interfacial interactions of ZrO_2 with the matrix, which can locally accelerate crystallization and modify growth kinetics. The contrast in behavior between TiO_2 and ZrO_2 thus suggests that while both reinforcements enhance tribological performance, their mechanisms of action differ: TiO_2 primarily contributes through load-bearing particle dispersion, whereas ZrO_2 actively tailors the microstructure by inducing crystallographic refinement. These findings provide valuable insight into the design of ceramic-reinforced Ni–B composites, indicating that the selection of reinforcement type is as crucial as its content in determining coating performance.

3.3. Microhardness

The incorporation of ceramic particles significantly enhanced the hardness of the coatings, with the effect depending on both reinforcement type and concentration. The microhardness values of plain Ni–B and TiO_2/ZrO_2-reinforced composite coatings are presented in Figure 7. The plain Ni–B coating exhibited a baseline hardness of approximately 750 HV, which is consistent with previously reported values for amorphous or nanocrystalline electroless Ni–B [10].

For both TiO_2 and ZrO_2 systems, hardness increased steadily with particle content up to 10 g/L. At this concentration, the maximum values were obtained: ~985 HV for TiO_2 reinforcement and ~1080 HV for ZrO_2 reinforcement, representing ~31% and ~45% improvements compared to plain Ni–B, respectively. The strengthening effect can be attributed to dispersion hardening and the load-bearing capacity of ceramic particles, which restrict dislocation motion and local plastic deformation [4]. At low reinforcement levels, the particles were homogeneously distributed within the matrix, enabling efficient stress transfer without disturbing structural continuity.

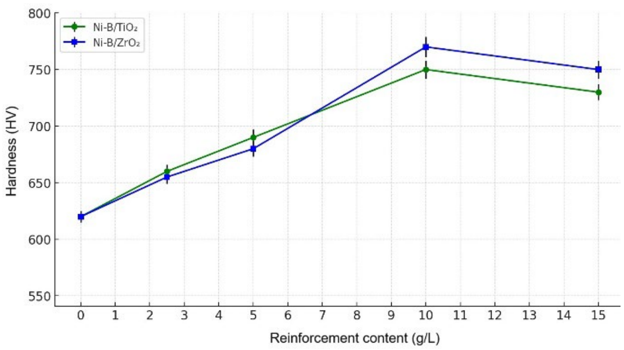

Figure 7. Vickers microhardness of Ni–B, Ni–B/TiO_2, and Ni–B/ZrO_2 coatings as a function of reinforcement content

At the highest reinforcement level (15 g/L), hardness values decreased slightly to ~900 HV (TiO_2) and ~950 HV (ZrO_2). This reduction is linked to particle agglomeration and clustering, which weakened matrix continuity and introduced microstructural heterogeneities, as also observed in SEM analyses. Such excessive particle loading creates brittle zones and stress concentration points, limiting further mechanical improvement.

When comparing the two reinforcements, both reinforcements contributed to enhancement of hardness; however, minor differences emerged depending on the type of reinforcement. XRD analysis showed that in TiO_2-reinforced coatings, the Ni peaks remained broad with only weak rutile reflections, confirming that TiO_2 acted mainly as an inert phase without altering the amorphous–nanocrystalline character of the Ni–B matrix. In contrast, ZrO_2-reinforced coatings exhibited sharper Ni (111) peaks together with distinct tetragonal and monoclinic ZrO_2 reflections (Fig. 6b). This indicates that ZrO_2 particles served as heterogeneous nucleation sites, promoting partial crystallization of the Ni–B matrix. The stronger interfacial interactions between ZrO_2 and the metallic matrix lowered the local energy barrier for crystal growth, which explains the formation of harder and more stable phases and the superior hardness values obtained with ZrO_2 [17–19].

These findings suggest an optimum reinforcement content of approximately 10 g/L, above which excessive particle addition leads to agglomeration and microstructural discontinuities that compromise coating integrity. This trend is in line with previous studies on particle-reinforced electroless coatings, which have consistently reported a critical concentration threshold where the beneficial effects of dispersion strengthening are offset by clustering and defect formation [4, 14, 24].

3.4. Tribological performance

The tribological behavior of Ni–B, Ni–B/TiO_2, and Ni–B/ZrO_2 coatings was evaluated under dry sliding against Al_2O_3 counterparts (Figure 8). For detailed wear testing, the coatings reinforced with 10 g/L particles were selected, as they exhibited both the highest hardness and the most favorable mechanical and tribological performance. The friction coefficient–distance profiles (Figure 8a) show that the plain Ni–B coating displayed an unstable curve, with a relatively high initial coefficient (~0.52) that increased further during sliding. This instability was primarily attributed to the absence of a protective tribofilm and the limited load-bearing capacity of the amorphous matrix, which promoted micro-deformation and adhesive wear. In contrast, TiO_2- and ZrO_2-reinforced coatings demonstrated lower and more stable friction coefficients throughout the test.

The TiO_2-reinforced coating displayed a steady coefficient of ~0.36, reflecting uniform particle distribution and stable surface interactions. The ZrO_2-reinforced coating initially showed the lowest coefficient (~0.32), although a slight increase occurred with sliding distance. This was attributed to localized particle detachment and third-body effects, where ceramic fragments acted as abrasive debris in the contact zone [4].

Although both reinforcements significantly improved tribological behavior, slight differences were observed in their dominant effects: TiO_2 reinforcement facilitated the formation of a continuous tribofilm and provided smoother sliding, thereby lowering and stabilizing the friction coefficient. In contrast, ZrO_2 reinforcement improved load-bearing capacity owing to its higher hardness and toughness, which enhanced resistance against material removal. These complementary effects explain why TiO_2-reinforced coatings exhibited lower friction coefficients, while ZrO_2-reinforced coatings showed lower wear rates [17–19].

The wear rates of the samples are summarized in Figure 8b. Ni–B exhibited the highest wear rate, while both TiO_2 and ZrO_2 additions substantially improved wear resistance. The lowest wear rate was measured for the ZrO_2-reinforced coating, confirming the beneficial effect of its higher hardness. However, the TiO_2-reinforced coating demonstrated more stable frictional behavior despite a slightly higher wear rate, suggesting that reinforcement type influences not only the overall wear resistance but also the consistency of tribological performance.

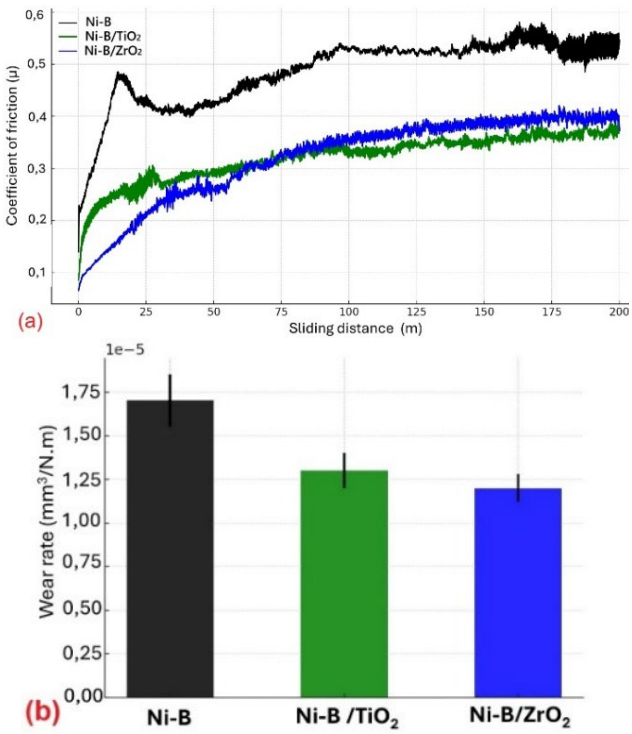

Figure 8. Tribological performance of Ni–B and composite coatings under dry sliding: (a) friction coefficient versus sliding distance, (b) wear rate comparison

3.5. Wear mechanisms

The SEM micrographs presented in Figure 9 provide insights into the microstructural reflections of the observed tribological behavior. In the case of the Ni–B coating (9a, 9d), pronounced wear tracks, microcracks, and delaminated regions were observed, indicating that the wear process was rather severe. Such surface morphology suggests the simultaneous operation of adhesive and intensive abrasive wear mechanisms. The formation of microcracks is attributed to repetitive surface stresses combined with the limited structural integrity of the amorphous matrix, eventually leading to material detachment from these regions.

For the TiO_2-reinforced coating (9b, 9e), the surface appeared smoother, with scratches progressing more uniformly and in parallel orientation, indicating improved microstructural continuity. This morphology points to a mechanism dominated by mild abrasive wear, where the embedded TiO_2 particles restricted deformation and stabilized the tribological contact.

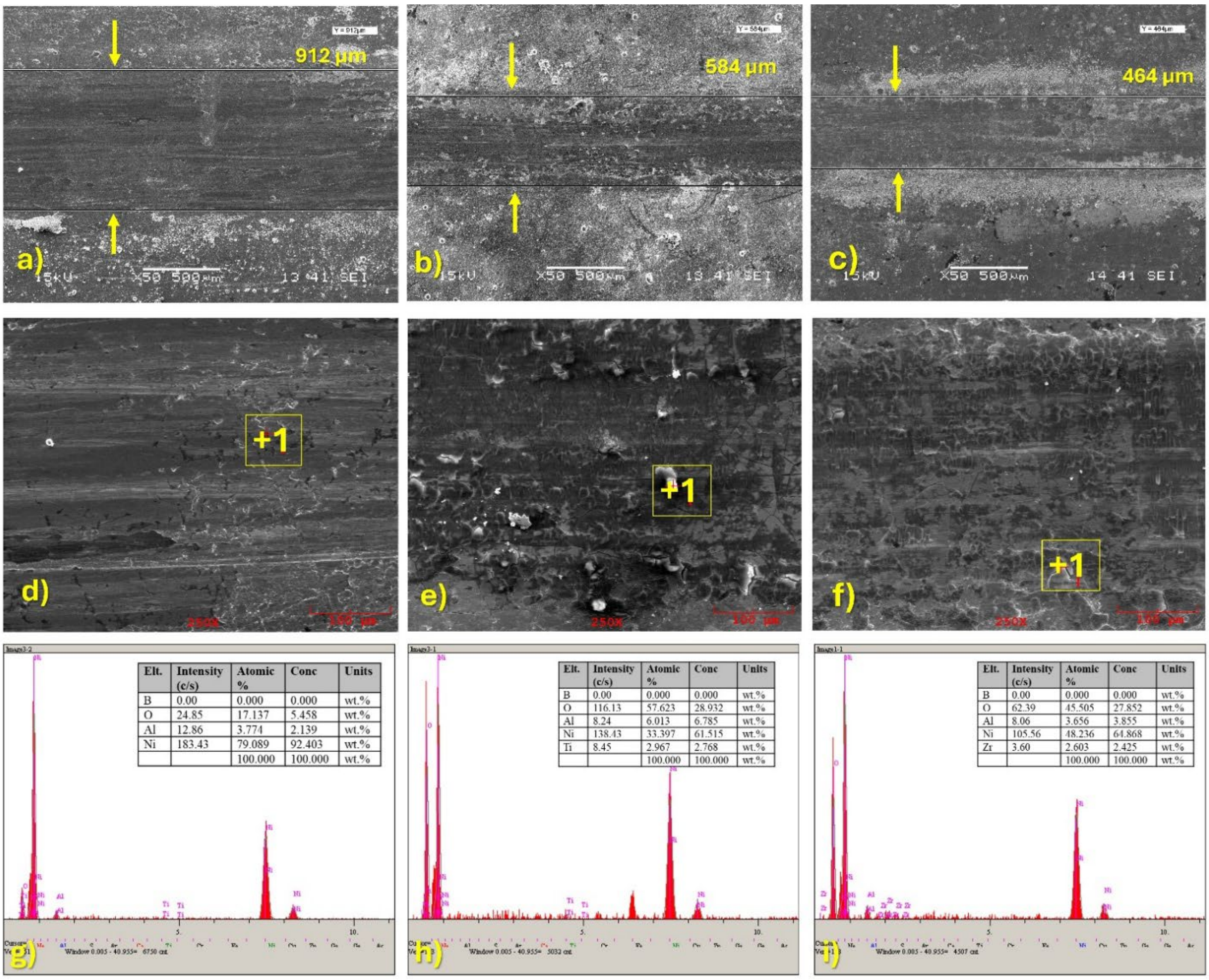

Figure 9. SEM micrographs and corresponding EDS analyses of worn surfaces after sliding tests: (a, d, g) plain Ni–B, (b, e, h) Ni–B/TiO_2, and (c, f, i) Ni–B/ZrO_2 coatings

The absence of significant tearing or cracking features confirms the enhanced load-bearing capacity of the composite.

In the ZrO_2-reinforced coating (9c, 9f), although the overall surface was relatively uniform, certain regions displayed particle accumulation, agglomeration, and localized surface disruptions. These features suggest that the tribological contact was occasionally destabilized by a third-body effect. Crack-like features observed at the microscale could be the consequence of the concentration of local stress.

Nevertheless, even with these minor instabilities, the high intrinsic hardness and toughness of ZrO_2 provided superior resistance to material removal, which explains the lowest wear rate observed among all coatings [17–19].

In summary, when Figures 8 and 9 are considered together, it becomes evident that while the Ni–B coating was dominated by destructive mechanisms such as severe wear and delamination, the incorporation of TiO_2 transformed these mechanisms into a more superficial and controlled form. On the other hand, ZrO_2 reinforcement provided higher hardness and lower wear rates, though minor particle-related irregularities introduced slight instabilities in the tribological response. These findings clearly demonstrate the potential of ceramic reinforcements to enhance the tribological performance of Ni–B coatings and highlight the critical importance of phase–matrix interactions in coating design.

The EDS spectra of the worn surfaces (Fig. 9g–i) confirm the influence of oxidative processes and counterface transfer on the wear behavior of the coatings. For the Ni–B sample, dominant Ni peaks together with strong oxygen signals and traces of Al indicated severe oxidative wear and material transfer from the Al_2O_3 ball, consistent with the unstable morphology observed in SEM. In contrast, the Ni–B/TiO_2 coating displayed clear Ti and O signals alongside Ni, verifying the retention of TiO_2 particles within the wear track. These reinforcements acted as load-bearing sites, reduced plastic deformation, and promoted more uniform contact. The Ni–B/ZrO_2 coating similarly exhibited Zr and O peaks, reflecting the stabilizing role of ZrO_2, although localized agglomeration led to minor instabilities. Overall, the EDS results demonstrate that while oxidative wear is common to all coatings, the incorporation of ceramic reinforcements—particularly TiO_2—significantly improves wear stability by enhancing surface integrity and mitigating severe degradation.

4. Conclusion

Electroless Ni–B and TiO_2/ZrO_2-reinforced composite coatings were successfully deposited. SEM and EDS analyses showed that plain Ni–B exhibited a typical nodular morphology, while ceramic particle addition gradually modified the surface. At low concentrations, particles were uniformly embedded, whereas higher contents led to clustering and heterogeneous topographies. XRD confirmed the amorphous–nanocrystalline structure of Ni–B, with TiO_2 acting mainly as an inert embedded phase and ZrO_2 promoting localized crystallization.

Microhardness results indicated that both reinforcements enhanced surface strength, with optimum hardness values of ~985 HV for TiO_2 and ~1080 HV for ZrO_2 at 10 g/L, representing ~31–45% improvement over plain Ni–B. Beyond this concentration, slight reductions occurred due to particle agglomeration. Tribological tests performed at the optimum content (10 g/L) revealed that TiO_2 provided lower and more stable friction coefficients, while ZrO_2 offered the best wear resistance owing to its higher hardness. Worn surface analyses confirmed that ceramic reinforcements transformed severe adhesive wear of plain Ni–B into milder abrasive mechanisms.

To conclude, the study confirms that ceramic reinforcements (TiO_2 and ZrO_2) play an important role in enhancing the hardness, wear resistance, and overall tribological performance of Ni–B coatings, while Pb-free processing ensures ecological compatibility. This dual advantage underscores their potential for surface engineering applications in automotive, aerospace, and tooling industries.

Article Information Form

Acknowledgments
This study was supported by the National Boron Research Institute of Türkiye (Project Number: 2017-31-07-25-001) and the Scientific Research Projects Unit of Sakarya University (Project Numbers: 2024-25-60-74).

The Declaration of Conflict of Interest/ Common Interest
No conflict of interest or common interest has been declared by the author.

Artificial Intelligence Statement
No artificial intelligence (AI) tools were used in the conception, data analysis, or writing of the scientific content of this study.

References

[1] V. B. Chintada, R. Koona, M. V. A. R. Bahubalendruni, “State of art review on nickel-based electroless coatings and materials,” Journal of Bio- and Tribo-Corrosion, vol. 7, no. 4, 2021.

[2] L. Magagnin, “Electroless deposition of Ni–P composite and multilayer coatings: Applications and perspectives,” ECS Meeting Abstracts, vol. MA2020-02(17), p. 1486, 2020.

[3] P. Sahoo, S. K. Das, “Tribology of electroless nickel coatings – A review,” Materials & Design, vol. 32, no. 4, pp. 1760–1775, 2011.

[4] D. Gültekin, E. Duru, H. Akbulut, “Improved wear behaviors of lead-free electroless Ni–B and Ni–B/CeO_2

composite coatings," Surface and Coatings Technology, vol. 422, p. 127525, 2021.

[5] X. Shu, Z. He, Y. Wang, L. Yin, "Mechanical properties of Ni-based coatings fabricated by electroless plating method," Surface Engineering, vol. 36, no. 9, pp. 944–951, 2019.

[6] K. S. Correia, L. G. Greca, L. Sopchenski, P. Soares, F. L. Amorim, R. D. Torres, "Strength and deformation properties of low-alloy steel bolts with electroless Ni–P coating: An investigation of two thermal routes," Journal of Materials Engineering and Performance, vol. 29, no. 9, pp. 6025–6032, 2020.

[7] T. S. N. S. Narayanan, I. Baskaran, K. Krishnaveni, S. Parthiban, "Deposition of electroless Ni–P graded coatings and evaluation of their corrosion resistance," Surface and Coatings Technology, vol. 200, no. 11, pp. 3438–3445, 2006.

[8] R. A. Shakoor, R. Kahraman, W. Gao, Y. Wang, "Synthesis, characterization and applications of electroless Ni–B coatings – A review," International Journal of Electrochemical Science, vol. 11, pp. 2486–2512, 2016.

[9] V. Vitry, F. Delaunois, "Development of electroless Ni–B coatings," Transactions of the IMF, vol. 93, no. 2, pp. 57–62, 2015.

[10] J. Sudagar, J. Lian, W. Sha, "Electroless nickel, alloy, composite and nano coatings – A critical review," Journal of Alloys and Compounds, vol. 571, pp. 183–204, 2013.

[11] S. Eraslan, M. Ürgen, "Oxidation behavior of electroless Ni–P, Ni–B and Ni–W–B coatings deposited on steel substrates," Surface and Coatings Technology, vol. 265, pp. 46–52, 2015.

[12] P. Gadhari, P. Sahoo, "Electroless nickel–phosphorus composite coatings," International Journal of Manufacturing, Materials, and Mechanical Engineering, vol. 6, no. 1, pp. 14–50, 2016.

[13] M. Yang, Y. Liang, T. Huang, Q. Jin, D. Kong, P. Song, "Oxidation behaviour and properties of carbide ceramic reinforced Ni-based composite coatings at 700 °C," Ceramics International, vol. 50, no. 20, pp. 37504–37517, 2024.

[14] P. Priyadarshi, P. K. Katiyar, R. Maurya, "A review on mechanical, tribological and electrochemical performance of ceramic particle-reinforced Ni-based electrodeposited composite coatings," Journal of Materials Science, vol. 57, no. 41, pp. 19179–19211, 2022.

[15] V. Niksefat, M. Ghorbani, "Mechanical and electrochemical properties of ultrasonic-assisted electroless deposition of Ni–B–TiO_2 composite coatings," Journal of Alloys and Compounds, vol. 633, pp. 127–136, 2015.

[16] E. Georgiza, A. Lekatou, D. Sioulas, A. E. Karantzalis, "SiC particle reinforced electroless Ni–B coatings and their tribological performance," Materials Chemistry and Physics, vol. 186, pp. 534–546, 2017.

[17] S. Mohanty, T. K. Barman, P. Sahoo, "Tribological behavior of TiO_2 reinforced Ni–B coatings," Coatings, vol. 13, no. 1, p. 145, 2023.

[18] H. Khaira, I. Shown, S. Samireddi, S. Mukhopadhyay, S. Chatterjee, "ZrO_2 reinforced Ni–B composite coatings for enhanced wear resistance," Journal of Materials Engineering and Performance, vol. 32, no. 2, pp. 1789–1802, 2023.

[19] C. C. Raidu, S. Boominathasellarajan, N. Arunachalam, "Tribological evaluation of ZrO_2 and YSZ nanoparticle reinforced electroless Ni–B coatings," Ceramics International, vol. 50, no. 9, pp. 15461–15471, 2024.

[20] S. I. Alnassar, H. M. Kadhim, S. R. Hassan, A. K. Mahmoud, A. A. A. G. Alrubaiy, "Synthesis of nano-SiC reinforced nickel-based nanocomposite coating using

electroless deposition technique," Materials Today: Proceedings, 2023.

[21] Y. Zhang, J. Zhang, "Synthesis of Ni, Cu plated nano-Al_2O_3 composite powders and autocatalytic mechanism," Materials Today Communications, vol. 38, p. 108178, 2024.

[22] F. Bülbül, A. Kara, "Multifunctional electroless nickel boron composite coatings incorporated by magnesium diboride ceramic particles," International Journal of Ceramic Engineering & Science, vol. 6, no. 6, 2024.

[23] V. Nemane, S. Chatterjee, "Evaluation of microstructural, mechanical, and tribological characteristics of Ni–B–W–SiC electroless composite coatings involving multi-pass scratch test," Materials Characterization, vol. 180, p. 111414, 2021.

[24] Y. Zhao, W. He, T. Zhang, "Microstructure and mechanical properties of Ni-based nanocomposite coatings: Effect of particle agglomeration," Journal of Materials Research and Technology, vol. 8, no. 5, pp. 4789–4797, 2019.

[25] G. Pedrizzetti, V. Genova, M. Bellacci, E. Scrinzi, A. Brotzu, F. Marra, G. Pulci, "Influence of deposition temperature and WC concentration on the microstructure of electroless Ni–P–WC nanocomposite coatings with improved hardness and corrosion resistance," Coatings, vol. 14, no. 7, p. 826, 2024.

[26] G. Jiaqiang, L. Lei, W. Yating, S. Bin, H. Wenbin, "Electroless Ni–P–SiC composite coatings with superfine particles," Surface and Coatings Technology, vol. 200, no. 20–21, pp. 5836–5842, 2006.

[27] Y. Yang, G. Wu, Y. Li, J. Liu, H. Wang, "Electroless Ni–P/nano-Al_2O_3 composite coatings," Applied Surface Science, vol. 257, no. 14, pp. 6113–6118, 2011.

[28] D. Ekmekçi, F. Bülbül, "Preparation and characterization of electroless Ni–B/nano-SiO_2, Al_2O_3, TiO_2 and CuO composite coatings," Bulletin of Materials Science, vol. 38, no. 3, pp. 761–768, 2015.

[29] F. Doğan, M. Uysal, H. Algül, E. Duru, H. Akbulut, S. Aslan, "Optimization of pulsed electro co-deposition for Ni–B–TiN composites and the variation of tribological and corrosion behaviors," Surface and Coatings Technology, vol. 400, p. 126209, 2020.

[30] E. Duru, F. Doğan, M. Uysal, H. Akbulut, S. Aslan, "Optimization of Ni–B coating bath and effect of DMAB concentration on hardness and wear," Surfaces and Interfaces, vol. 22, p. 100880, 2021.

[31] A. Kumar, A. Mukhopadhyay, "Investigation of Ni–Cu–B and Ni–Cu–Sn–B coatings developed by electroless method," Journal of the Indian Chemical Society, vol. 100, no. 11, p. 101102, 2023.

[32] N. S. Qu, L. Q. Zhang, Z. X. Wang, D. Zhu, "Properties of Ni–CeO_2 composite coatings obtained by electrodeposition," Surface Engineering, vol. 22, no. 3, pp. 173–176, 2006.